HardwareX 4 (2018) e00030

Contents lists available at ScienceDirect

HardwareX

journal homepage: www.elsevier.com/locate/ohx

Hardware Article

Implementation of a flexible, open-source platform for ion mobility spectrometry

Tobias Reinecke, Brian H. Clowers *

Department of Chemistry, Washington State University, Pullman, WA 99164, United States

ARTICLE INFO

Article history:
Received 2 April 2018
Received in revised form 8 May 2018
Accepted 9 May 2018

Keywords:
Ion mobility spectrometry
Chemical instrumentation
Laboratory instrumentation
Trace analysis

ABSTRACT

When operated as a stand-alone device, an ion mobility spectrometer (IMS) routinely offers low limits of detection (pptv-range) for gas-phase analytes even for measurement times less than a second. Mass analyzers further enhance the analytical power of IMS separations, however, high performance drift-cell IMS instruments are often highly customized, relatively large, and require extensive expertise to operate. In this work we present an optimized, low cost IMS system that leverages an easy-to-assemble ion gating structure that enables IMS spectra with resolving powers exceeding 90 for a drift cell only 10 cm in length. The IMS presented in this work consists of stacked rings divided by spacers all fabricated from printed circuit boards (PCB). The rings are connected via a slotted PCB-board containing a surface mounted voltage divider that connects directly to the ring electrodes allowing a fast and easy assembly. This highly modular design enables e.g. the realization of variable drift tube lengths or single and dual gate setups. Instead of the commonly used Bradbury Nielsen gates, the IMS is equipped with a 3-grid ion gate allowing the generation of short (<50 μs) ion packets increasing the resolving power of the instrument.

Specifications table

Hardware name	Ion Mobility Spectrometer
Subject area	• Chemistry and Biochemistry • Environmental, Planetary and Agricultural Sciences • Educational Tools and Open Source Alternatives to Existing Infrastructure • General
Hardware type	• Measuring physical properties and in-lab sensors • Biological sample handling and preparation • Field measurements and sensors • Electrical engineering and computer science • Mechanical engineering and materials science
Open Source License	CERN OHL v.1.2 (https://www.ohwr.org/licenses/cern-ohl/license_versions/v1.2)
Cost of Hardware	~$210 USD for the PCB-IMS and high speed, high gain amplifier
Source File Repository	OSF Link: https://osf.io/p6d4x/Github: https://github.com/bhclowers/OS-IMS

* Corresponding author.
E-mail address: brian.clowers@wsu.edu (B.H. Clowers).

https://doi.org/10.1016/j.ohx.2018.e00030
2468-0672/

Warning: Exercise extreme caution when operating and working around the PCB IMS system. Be vigilant regarding the voltage potentials used and the current necessary to drive the unit. Establish appropriate engineering controls to shield the system.

To operate the described PCB IMS it needs to be connected to a high voltage power supply. During operation, conductors at dangerous voltages may be exposed. Extreme care should be taken to protect against shock. Stand on an insulating pad and use only one hand when checking components. Always work with another person in case an emergency occurs. Any work on an operational system should only be executed after the high voltage connectors have been disconnected and the power deenergized.

1. Hardware in context

Ion mobility spectrometry is a gas-phase separation technique that finds utility across analytical domains [1–4]. Most notably, this technique supports many of the field-based detection platforms used to screen passengers, baggage, and goods for explosives and narcotics [5]. Select IMS instruments also find extensive use as point detectors for chemical warfare agents [6]. The wide use of IMS in the field is largely predicated on its relative speed, chemical selectivity, and capacity to operate without expensive vacuum pumps. The sensing principle of IMS is based on a separation of ions by their ion-specific velocity in a drift gas under the influence of an electric field. Compared to other laboratory approaches that probe gas-phase ions, such as mass spectrometry [7], ion mobility systems currently have yet to realize the same levels of resolution. Nevertheless, they serve a critical role as a screening tool. It is important to recognize that the primary role of devices such as IMS is to minimize false negatives where such outcomes are untenable. From a fundamental science perspective, IMS devices also serve as key tools for probing ion-neutral interactions, gas-phase chemistry, and thermodynamic properties of clusters not accessible using other approaches [7–10].

Despite their wide deployment and importance to fundamental science, there are few literature reports detailing the construction and operation of a high-performance, drift-tube ion mobility system. For reference, there are a range of analytical techniques that exploit the property of gas-phase ion mobility to separation ions but the drift tube system arguably provides the largest degree of flexibility, resolution, and accuracy. Conceptually, drift-tube IMS hardware is simple but construction of such devices that produce consistent results has proven challenging and often relied upon a select set of skills, access to resources, and tribal knowledge. In its simplest form, drift tube IMS systems are comprised of an ionization source, reaction/desolvation region, ion gate, drift cell, and detector. Supporting components also include a stable high voltage power supply, ion gating electronics, and a high speed, high-gain current to voltage converter. In the present embodiment of the drift tube IMS, we detail an easily manufactured, open-source drift tube design that incorporates a robust 3-grid shutter design that greatly eases assembly and still enhances performance compared to the traditionally used Bradbury Nielsson Ion gate [11]. In order to maximize the analytical performance, the design process for the size of electrodes, spacers and detector followed the general guidelines given by Bohnhorst et al. [12]. As demonstrated in the latter sections of this report, the IMS system used in this report is capable of attaining resolving powers above 90 for a 10 cm drift cell which exceeds the performance of most commercial systems with a similar footprint. Additional IMS elements included in this design are the drift gas inlet (used to control the local gas-phase environment), detector assembly, and a high-speed, high-gain current to voltage converter. Though a control system is left to the user (a traditional oscilloscope will often suffice), we make recommendations and provide guidance on such tools. It should also be noted that another key element of the drift-tube IMS system not covered in this communication is the ion gate pulser. However, in a separate report [13], we detail the operation and performance of an open-source unit capable of supplying that information.

2. Modular drift tube description and assembly

In this section the assembly of the PCB desolvation and drift region as shown in Fig. 1 is described. In a first step, the electrode alignment board (Fig. 2) is equipped with resistors, specifically surface mount 1206 components. For the presented IMS, 1 MΩ ± 1% resistors were used, but more important than the value of the resistor is to consider sufficient voltage ratings. A 10.4 cm drift tube (or desolvation region respectively) consists of 29 electrodes (Fig. 3) and 56 spacers (Fig. 4).

The distance between two electrodes and the inner diameter of the ring electrodes and spacers were chosen according to Bohnhorst et al. in order to realize a homogeneous electric field inside the drift tube enabling to utilize ions within 90% of the inner electrode radius [12]. These design consideration allow the size of the detector to be maximized without broadening of the ion peaks due to field inhomogeneities in close proximity to the electrodes. Therefore, this design leads to an optimum balance between sensitivity and resolving power.

The electrodes and spacers are stacked on rods (we used poly ether ether ketone (PEEK) rods with a 6 mm diameter and threaded ends though any appropriate, non-conducting material would suffice), beginning with an electrode followed by two spacers as shown in Fig. 5. This alternating pattern of 2 spacers to 1 electrode is repeated to achieve the desired drift cell length. Finally, the electrode alignment board is set on top of the stack and the electrode contacts are soldered to the connectors on the alignment board. To achieve higher stability of the setup it is advantageous to connect a second electrode alignment board without resistors to the bottom of the stack. To prevent misalignment of the electrodes and spacers, soldering of the electrode alignment board should only be conducted when the spacers and electrodes are aligned on the

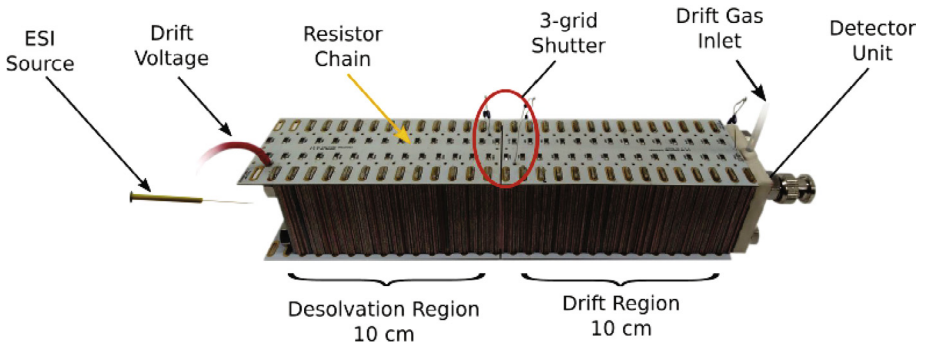

Fig. 1. Photo of the PCB-IMS assembly. Labeled are the pertinent components needed for operation. Details for all of the components, aside from the ion source (as that can vary depending on upon the application) are detailed in this communication.

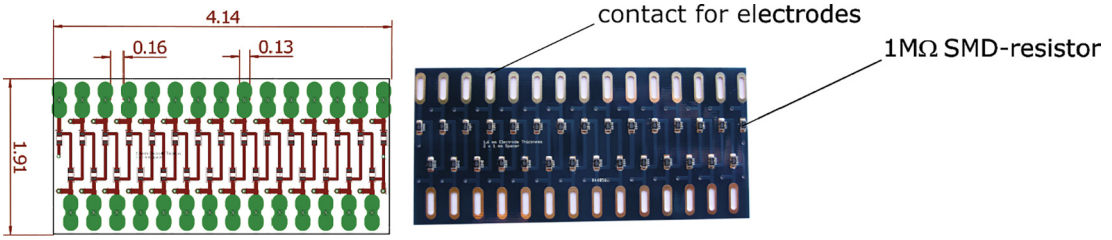

Fig. 2. Schematic and photo of the electrode alignment board. The layout of this board connects each subsequent electrode into a resistor chain established by the surface mount resistors.

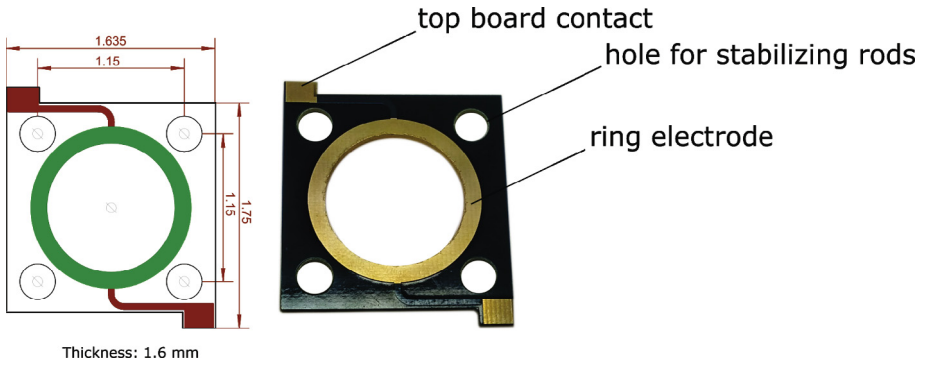

Fig. 3. Schematic and photo of an electrode used to realize a homogeneous electric field inside the drift tube.

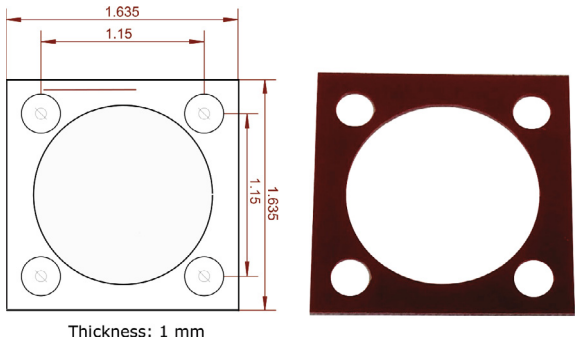

Fig. 4. Schematic and photo of a spacer used to distance two electrodes.

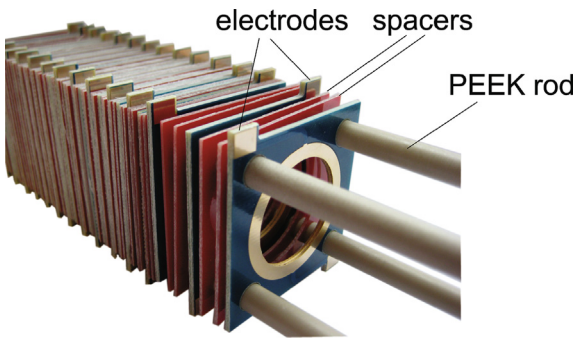

Fig. 5. Stack of electrodes and spacers on centering PEEK rods.

previously described alignment rods. It should be noted, that the PCB manufacturing process and soldering may create a dirty system. Therefore it is important to clean the drift tube to enable the measurement of clean spectra. Isopropanol was used to clean the parts and subsequently placed the assembled drift tube in a vacuum oven at elevated temperature (180 °F). It is also worth mentioning that the spacing of the electrodes was chosen to optimize the homogeneity of the resulting electric field when connected to a resistive divider. However, upon assembly the system is not necessarily air tight. To seal the system a higher degree of compression would be needed along with a different top board (Fig. 2.). Nevertheless, with a positive pressure of gas moving through the system the gas within the cell may be kept relatively clean. If a particular experiment requires a sealed system it is surely possible to place the system within a second enclosure.

2.1. 3-Grid ion shutter

To inject short ion packages from the desolvation region into the drift region, an ion shutter is necessary. A commonly used ion shutter is the Bradbury Nielsen ion gate [15]. It consists of a parallel set of wires, which are set to opposite potentials in order to create a field orthogonal to the drift field and thus stopping the ions from entering the drift region. However, as the manufacturing of this type of gate is time and resource intensive, not to mention extreme levels of patience, we employ a different type of ion shutter which was first introduced by Langejuregen et al. and shown to provide favorable levels of performance for electrospray ion mobility spectrometry [14,16]. Fig. 6 depicts a schematic of the employed

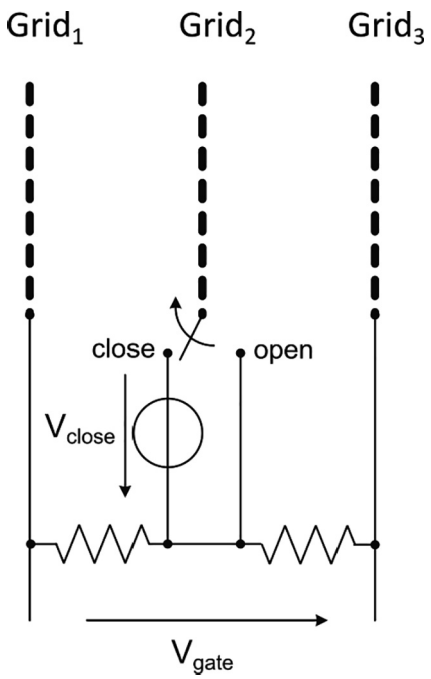

Fig. 6. Schematic of the 3-grid ion shutter. Compared to the traditional ion gate, the static grid structure eases assembly and operation [14]. In the open state the potential of the center grid ($Grid_2$) is held at a value equal to the center potential between $Grid_1$ and $Grid_3$. The gating electronics are detailed in a separate manuscript and allow for the modulation of this floated potential [13].

3-grid ion shutter. It consists of 3 grids separated by spacers. $Grid_1$ and $Grid_3$ are connected via two equal resistors. To realize a field in the open shutter equal to the field in drift and desolvation region, the used resistors should have a value of 150 kΩ, when using 1 MΩ on the electrode alignment board. When the gate is open, $Grid_2$ is connected to the center potential between $Grid_1$ and $Grid_3$, creating a field gradient that is allowing ions to pass from desolvation region to drift region. To close the gate, $Grid_2$ is connected to a higher potential and therefore the electric field between $Grid_1$ and $Grid_2$ is reversed and stopping the ions from entering the drift region while the field in drift and desolvation region stays constant as the potential on $Grid_1$ and $Grid_3$ remains unchanged. The voltage necessary to stop the ions depends on the field strength in the ion gate and typically ranges between 30 V and 80 V. It can be advantageous to stabilize the voltage on $Grid_1$ and $Grid_3$ with a capacitor (capacitor gate 4700 pF 10 kV) connected to the respective gate and ground.

Fig. 7 shows the stainless steel grid we used to implement the 3-grid ion shutter. The thickness of the grid is 0.1 mm and was produced in a photo chemical etching process by *Newcut* (Newark, NY). Fig. 8 shows a photo of the 3-grid shutter. $Grid_1$ is in direct contact with the last electrode of the desolvation region. Then a 300 μm PTFE spacer is inserted, followed by $Grid_2$, another PTFE spacer and $Grid_3$. For reference the PTFE spacer can be constructed using a pair of scissors and a ¼" hole punch, or for those more enterprising, an electronic scrapbook cutter. The footprint of each PTFE spacer conforms to the standard 1 mm PCB spacer detailed in Fig. 4.

2.2. Integrated Faraday detector and drift gas inlet

The detector consists of a Faraday plate enclosed by a ground plane, see Fig. 9. To enable an evenly distributed flow of drift gas over the cross section of the drift tube, the Faraday plate is surrounded by pinholes which serve as drift gas inlets. On the backside, the Faraday plate is connected to the inner conductor of an SMA connector and the ground plane to the outer conductor respectively. To realize a connection from the detector to the drift gas supply, 3 spacers with a small cut-out are stacked on the backside of the detector, as shown in Fig. 10. Subsequently, a 1/16″ ID Teflon hose is placed in the cutout. As depicted in Fig. 11, the backplate is then placed on the stack of spacers and sealed with an O-ring. Finally, the Teflon hose is glued in for better seal and stability. Note that it is important to use an adhesive with low vapor pressure in order to keep the drift gas free from contamination. A suitable choice is *TorrSeal*.

To shield the detector from an image current induced from the approaching ion cloud, the drift tube is terminated with an aperture grid which is directly placed on the last electrode, followed by 1 spacer and finally the detector. The aperture grid is

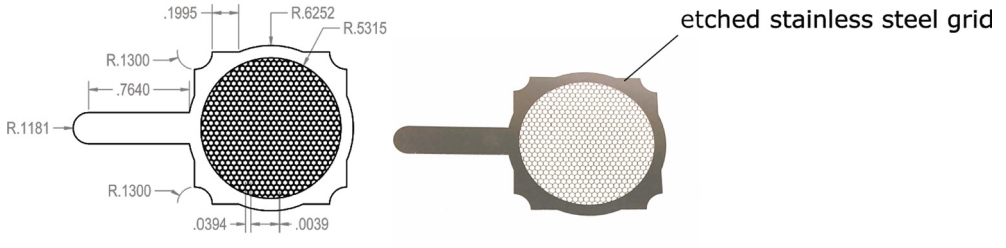

Fig. 7. Schematic and photo of the etched stainless steel grid.

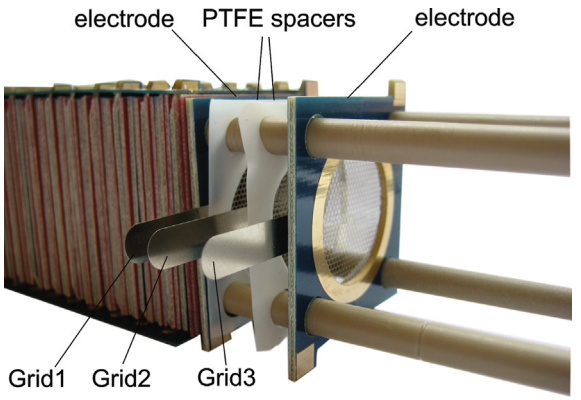

Fig. 8. Photo of the 3-grid ion shutter.

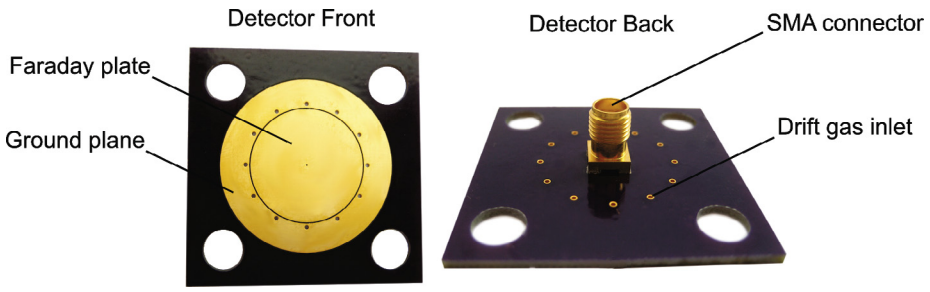

Fig. 9. Faraday plate with SMA-connector.

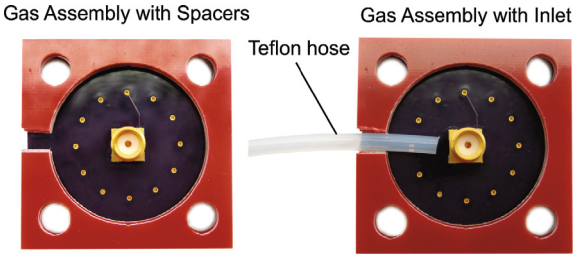

Fig. 10. Spacers are stacked on the backside of the detector and a Teflon hose is put in place.

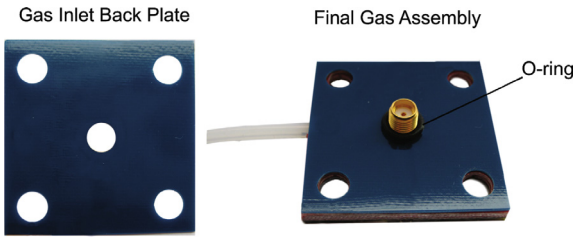

Fig. 11. The detector is sealed with a backplate and O-ring.

connected via a 500 kΩ resistor to ground, as shown in Fig. 12. To stabilize the voltage on the aperture grid, it is advantageous to add an additional capacitor (we used 0.22 μF) in parallel to the resistor.

2.3. Amplifier

To amplify the current produced by the ions discharging on the Faraday plate, a transimpedance (current to voltage) amplifier is necessary. The amplifier described in this section is shown in Fig. 13. It has a variable gain that can be set to either 10^8 or 10^9.

The Schematic is depicted in Fig. 14. To achieve the maximum gain, this amplifier uses two stages. Stage 1 consisting of an operational amplifier and the resistor R1 provides a current-to-voltage amplification of R1 = 10^8 Ω. The resistor R2 was added to protect the input of the operational amplifier. However, it might not be necessary to use R2. When the switch is set to "1e8" (as depicted in the schematic), the output signal of Stage 1 is fed to Stage 2a which only consists of 1 operational amplifier (A) and resistor R6. The output of this operational amplifier is directly fed back to the negative input leading to an amplification of 1 and thus to an overall amplification of 10^8. However, Stage 2a acts as a voltage follower (buffer amplifier) to achieve an amplifier performance that is independent of the current drawn from the load (in this case the data acquisition system). When the switch is set to "1e9", the output signal of Stage 1 is fed to Stage 2b. Under this scenario, the output voltage of the operational amplifier (B) is divided by the voltage divider consisting of R3, R4 and R5 to (R3||R5)/((R3||R5) + R3) = 1/10 and fed back to the negative input of (B). Thus, an additional amplification of 10 is realized leading to an overall amplification of 10^9. The rise time of the amplifier critically depends on the input capacitance, but in normal operation a rise time of approximately 20 μs is easily achievable which is sufficient to amplify the ion current without adding significant broadening to the ion peak.

3. Design files summary

Primary Source Location: https://github.com/bhclowers/OS-IMS/tree/master/PCB_IMS

Design file name	File type	Open source license	Location of the file
1a_Spacers.brd	Eagle file	CERN OHL v1.2	https://github.com/bhclowers
1b_Spacer.STL	STL file	CERN OHL v1.2	https://github.com/bhclowers
2a_Electrodes.brd	Eagle file	CERN OHL v1.2	https://github.com/bhclowers
2b_Electrode.STL	STL file	CERN OHL v1.2	https://github.com/bhclowers
3_electrode alignment board.brd	Eagle file	CERN OHL v1.2	https://github.com/bhclowers
4_Detector.brd	Eagle file	CERN OHL v1.2	https://github.com/bhclowers
5_detector backplate.brd	Eagle file	CERN OHL v1.2	https://github.com/bhclowers
6_Grid.STL	STL file	CERN OHL v1.2	https://github.com/bhclowers
7_schematic amplifier.dch	diptrace file	CERN OHL v1.2	https://github.com/bhclowers
8_layout amplifier.dip	diptrace file	CERN OHL v1.2	https://github.com/bhclowers
9_amplifier_gerbers.zip	Zipped Gerber Files	CERN OHL v1.2	https://github.com/bhclowers

4. Bill of materials

Designator	Component	Quantity	Cost per unit USD	Total cost	Source of materials
	Amplifier			$62.60	
Fig. 13	DIODE SCHOTTKY	2	$0.41	$0.82	Digikey
Fig. 13	Capacitor 0.1UF 50 V X7R RADIAL	4	$0.18	$0.72	Digikey
Fig. 13	Capacitor 100PF 3KV NP0 RADIAL	1	$2.77	$2.77	Digikey
Fig. 13	Capacitor TANT 47UF 6.3 V 10% RADIAL	2	$1.03	$2.06	Digikey
Fig. 13	IC OPAMP JFET 1MHZ 8SO	1	$5.13	$5.13	Digikey
Fig. 13	IC OPAMP GP 1MHZ 8SOIC	1	$8.00	$8.00	Digikey
Fig. 13	SWITCH SLIDE DPDT 50MA 48 V	1	$2.90	$2.90	Digikey
Fig. 13	BNC JACK R/A 50 OHM PCB	2	$3.48	$6.96	Digikey
Fig. 13	Resistor 100 M OHM 1/4W 1% AXIAL	1	$4.63	$4.63	Digikey
Fig. 13	Resistor 10 K OHM 1/4W 1% AXIAL	3	$0.10	$0.30	Digikey
Fig. 13	Resistor 1.13 K OHM 1/4W 1% AXIAL	1	$0.56	$0.56	Digikey
Fig. 13	Resistor 9.09 K OHM 0.6 W 1% AXIAL	1	$0.29	$0.29	Digikey
Fig. 13	Resistor 6.65 K OHM 1/2W 1% AXIAL	1	$0.61	$0.61	Digikey
Fig. 13	AC/DC CONVERTER ±15 V 6 W	1	$22.05	$22.05	Digikey
Fig. 13	PCB Board			$4.80	OSHPark
	2 × 10 cm *Drift Tube including detector*			$148.48	
Fig. 4	Spacers	116	$0.30	$34.80	DirtyPCBs
Fig. 3	Electrodes	58	$0.35	$20.30	DirtyPCBs
Fig. 7	Grids	4	$10.00	$40.00	Newcut
Fig. 2	electrode alignment board	2	$3.40	$6.80	DirtyPCBs
Fig. 9	detector board	1	$4.45	$4.45	OSHPark
Fig. 11	detector back plate	1	$0.30	$0.30	OSHPark
Fig. 5	rods	4	$2.00	$8.00	McMaster
	capacitor aperture grid (.22uF 2000 V 10%)	1	$4.65	$4.65	Mouser
	capacitor gate (optional) 4700pF 10 kVolts	2	$4.84	$9.68	Mouser
	capacitor HV (optional) 2500pF 15 kVolts	1	$6.16	$6.16	Mouser
Fig. 2	Resistors SMD 1 M Ohm 1/4W 1206	58	$0.23	$13.34	Digikey

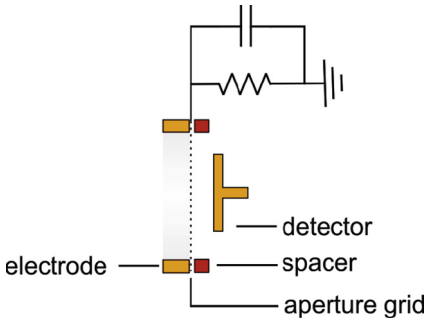

Fig. 12. Schematic of the connected aperture grid.

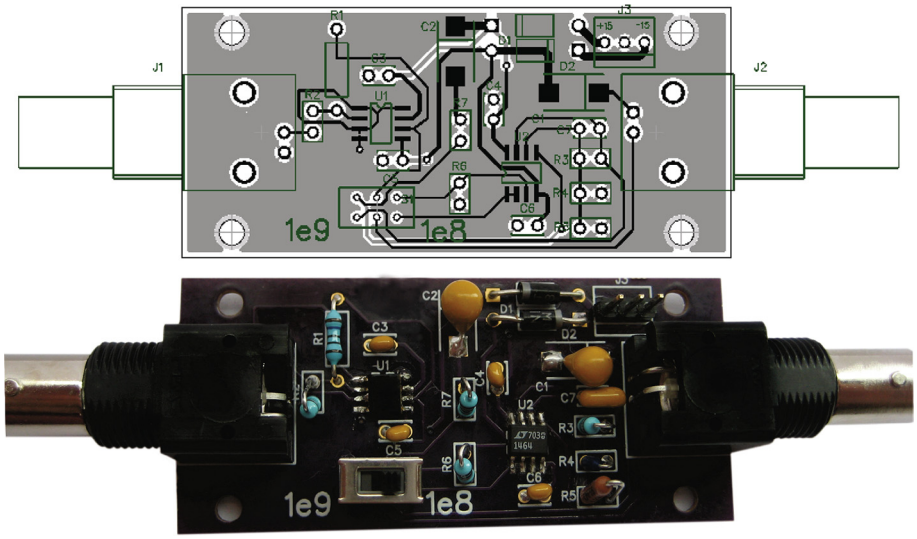

Fig. 13. PCB layout and photo of the high-speed, high-gain transimpedance amplifier.

5. Operation instructions

Once assembled and tested electrically (i.e. the resistance is appropriate across the voltage divider, grids in the ion shutter are not short circuited, aperture grid is not touching the detector) a high voltage source may be applied to the 1st electrode of the electrode alignment board. Though outside the scope of this hardware description, a high voltage power supply is necessary for the correct operation of the PCB-IMS. With 29 electrodes per 10 cm, the resistor chain for a 20 cm cell is approximately 58 MΩ which requires 160–200 μA at 10–12 kV to achieve an electric field strength of 500–600 V/cm.

Prior to operation the following checklist should be followed (at a minimum):

- Sufficient clearance is provided from other conductive surfaces to avoid high voltage discharge.
- Ensure that a source of clean-dry drift gas (e.g. air or nitrogen) is present flowing over the detector at a rate of 200–500 mL/min.
- Power is connected to the transimpedance amplifier and the unit is operational.
  - o Testing of the amplifier can e.g. be performed by applying a voltage of 1 V over a 100 MΩ at the input (i.e. input current of 10^{-9}A) and checking if an output voltage of 1 V can be measured when the amplification is set to "1e9" and an output voltage of 0.1 V when the amplification is set to "1e8" respectively.
- The resistors comprising the voltage divider are secured and the appropriate resistances are measured between electrodes.
- A resistor of approximately 500 kΩ is placed between the aperture grid and ground.
- No electrical connection exists between $Grid_1$ and $Grid_2$ and $Grid_2$ and $Grid_3$.
  - o Altering the potential of Grid2 is the primary mechanism of modulating the ion beam.
  - o Operation of the IMS in an open mode can be achieved by placing $Grid_2$ in the resistor chain of the system at the potential midway between $Grid_1$ and $Grid_3$.

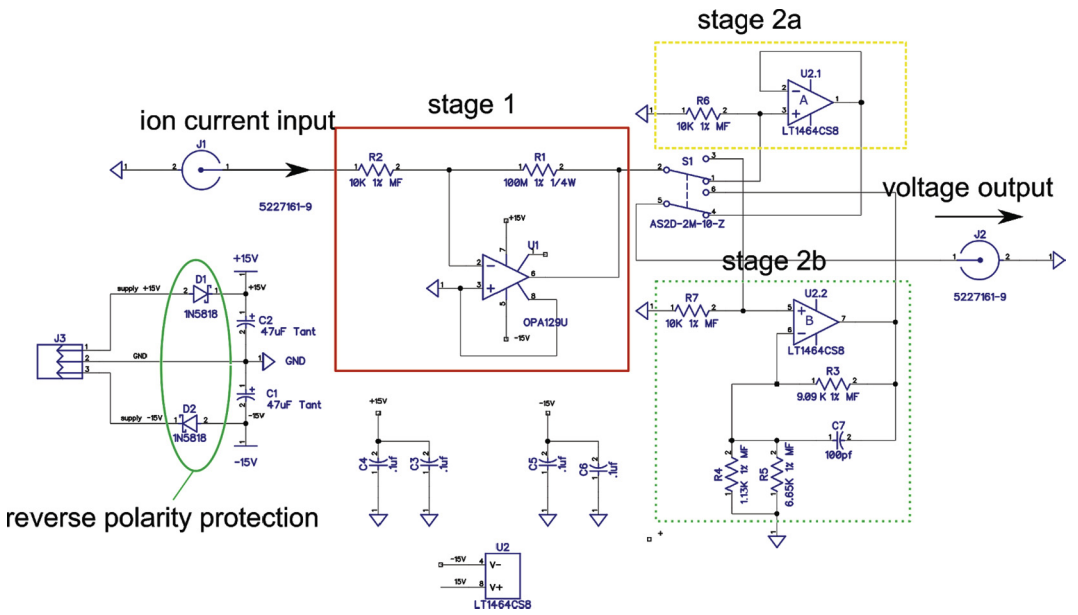

Fig. 14. Schematic of the of the high-speed, high-gain transimpedance amplifier.

- If possible, limit the current output of the high voltage power supply only to the value needed for safe operation.
  - o Recognizing that high voltage itself is not necessarily dangerous, extreme caution is advised when using high voltage power supplies capable of delivering such levels of current. Prior to operation, it is advised that those unfamiliar with such hardware contact a subject matter expert or their organization's electrical safety officer to ensure proper engineering controls are in place.

A range of different ionization sources are compatible with ion mobility spectrometry. On a fundamental level the source of the ions is not as important but the simple fact that ions are produced in a reproducible fashion. Relevant examples include ^{63}Ni [17], ^{3}H [18], corona discharge [19], micro-plasma [20], electron sources [21], x-rays [22], and electrospray ionization (ESI) [23].

Though radioactive sources are widely deployed, their use requires appropriate safety and licensing and are not recommended unless there is a specific need. For initial experimentation, a corona discharge can be employed. A standard corona source can be made by using any reasonably sharp metal pin located ~1 cm from the first electrode and biased 3–4 kV *above* that entrance potential. As Fig. 15 illustrates, the ion gates may be toggled in an on an off fashion using the electronics referenced previously [13]. It is worth noting that when measuring positive ions using the system the transimpedance amplifier

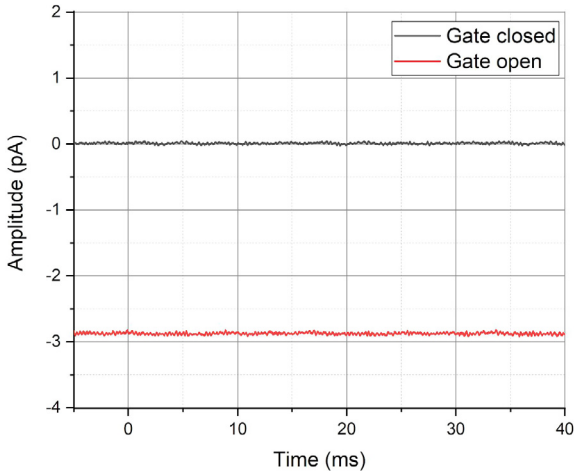

Fig. 15. Measured spectrum for an continuously open and closed ion gate.

will register a negative voltage and the opposite is true for negative ions. Alternatively, it is simple enough to test whether the system remains in an operational state with respect to measuring ion current simply by turning the ion source on and off while the gate is held open.

6. Validation and characterization

The first ring of the desolvation region was connected to an electric potential of 11.5 kV via a high voltage power supply. To stabilize the drift voltage, an additional capacitor (capacitor HV 2500pF 15 kV) was connected in parallel to the complete IMS system. The drift gas inlet on the detector was connected to a supply of purified nitrogen. The flow rate was set to 0.5 L/min via a mass flow controller (a simple ball meter can also suffice). The detector of the IMS is connected to the amplifier. For data acquisition and generation of the trigger pulse for the pulse generator we used an *Analog Discovery* (Digilent, Pullman, WA) unit. The pulse width of the injection pulse was set to 50 μs. For the measurement of the corona-ionization spectrum (Fig. 17(a)), a home built corona needle was placed centric and in close proximity to the first ring of the desolvation region and connected to an electric potential of 14.5 kV. Then, sampled headspace from 2,4-lutidine was applied via a PEEK

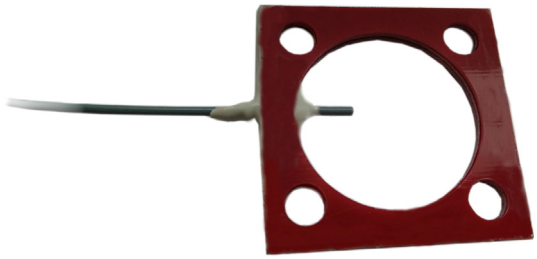

Fig. 16. Capillary inlet for gaseous samples.

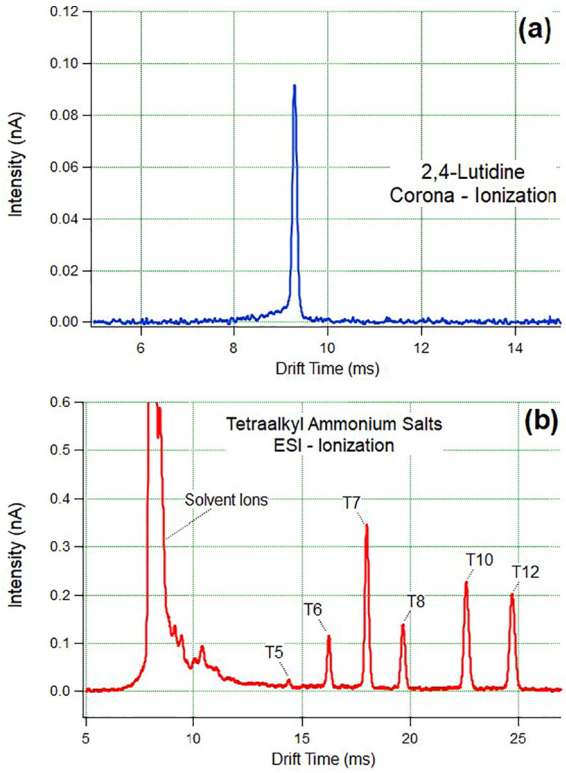

Fig. 17. Representative spectra obtained using the PCB IMS. The top spectrum (a), corresponds to the peaks observed for the headspace from a 2,4-lutidine sample ionized using a corona needle. The lower spectrum (b), corresponds to a series of tetraalkylammonium salts electrosprayed at room temperature. The resolving powers (i.e. peak centroid divided by peak width at half height) for the two spectra range from R = 82 (Corona spectrum) to R = 92 (ESI spectrum).

capillary which is connected to a gas tight syringe containing the sample. The capillary sample inlet is shown in Fig. 16. The assembly is similar to the assembly of the drift gas inlet described above, while using a 0.01 ID/0.062 OD PEEK capillary instead of the Teflon hose. Due to the smaller diameter of the capillary compared to the Teflon hose, only one (middle) of the three spacers used has a cut out. It should be noted that a range of gas-phase sample introduction mechanisms may be implemented.

For the measurement of the ESI spectrum (Fig. 17(b)), the corona needle was replaced by an ESI needle which was then connected to a potential of 13.5 kV. A 12 μM solution of a series of tetraalkylammonium salts was then supplied with a syringe pump and a flow rate of 5 μL/min. The resolving powers (i.e. peak centroid divided by peak width at half height) for the two spectra range from R = 82 (Corona spectrum) to R = 92 (ESI spectrum).

Declaration of interest

B.H. Clowers is a co-inventor of a number of patents (US-2009294662-A1, US-2007158543-A1, US-2013260478-A1, US-2017074826-A1, US-2017023453-A1) related to ion mobility spectrometry, however, the present report does not infringe on those disclosures.

Acknowledgement

We would like to acknowledge support from the NSF under award CHE-1506672.

Appendix A. Supplementary data

Supplementary data associated with this article can be found, in the online version, at https://doi.org/10.1016/j.ohx.2018.e00030.

References

[1] G.A. Eiceman, Z. Karpas, H.H. Hill Jr., Ion Mobility Spectrometry, third ed., CRC Press, 2013.
[2] X. Zhang, K. Quinn, C. Cruickshank-Quinn, R. Reisdorph, N. Reisdorph, The application of ion mobility mass spectrometry to metabolomics, Curr. Opin. Chem. Biol. 42 (2018) 60–66.
[3] I.D.G. Campuzano, J.L. Lippens, Ion mobility in the pharmaceutical industry: an established biophysical technique or still Niche?, Curr Opin. Chem. Biol. 42 (2018) 147–159.
[4] K.A. Morrison, B.H. Clowers, Contemporary glycomic approaches using ion mobility–mass spectrometry, Curr. Opin. Chem. Biol. 42 (2018) 119–129.
[5] R.G. Ewing, D.A. Atkinson, G.A. Eiceman, G.J. Ewing, A critical review of ion mobility spectrometry for the detection of explosives and explosive related compounds, Talanta 54 (3) (2001) 515–529.
[6] M.A. Mäkinen, O.A. Anttalainen, M.E.T. Sillanpää, Ion mobility spectrometry and its applications in detection of chemical warfare agents, Anal. Chem. 82 (23) (2010) 9594–9600.
[7] S. Kim, R.P. Rodgers, A.G. Marshall, Truly, "exact" mass: elemental composition can be determined uniquely from molecular mass measurement at ~0.1mda accuracy for molecules up to ~500Da, Int. J. Mass Spectrom. 251 (2–3) (2006) 260–265.
[8] K. Giles, E.P. Grimsrud, The kinetic ion mobility mass spectrometer: measurements of ion-molecule reaction rate constants at atmospheric pressure, J. Phys. Chem. 96 (16) (1992) 6680–6687.
[9] P. Kwantwi-Barima, H. Ouyang, C.J. Hogan, B.H. Clowers, Tuning mobility separation factors of chemical warfare agent degradation products via selective ion-neutral clustering, Anal. Chem. 89 (22) (2017) 12416–12424.
[10] H.E. Revercomb, E.A. Mason, Theory of plasma chromatography/gaseous electrophoresis. Review, Anal. Chem. 47 (7) (1975) 970–983.
[11] A.T. Kirk, S. Zimmermann, Bradbury-Nielsen vs. field switching shutters for high resolution drift tube ion mobility spectrometers, Int. J. Ion Mobil. Spec. 17 (3-4) (2014) 131–137.
[12] A. Bohnhorst, A.T. Kirk, S. Zimmermann, Simulation aided design of a low cost ion mobility spectrometer based on printed circuit boards, Int. J. Ion Mobil. Spectrom. 19 (2–3) (2016) 167–174.
[13] L. Garcia, C. Saba, G. Manocchio, G.A. Anderson, E. Davis, B.H. Clowers, An open source ion gate pulser for ion mobility spectrometry, Int. J. Ion Mobil. Spectrom. 20 (3–4) (2017) 87–93.
[14] T. Reinecke, A.T. Kirk, A. Ahrens, C.-R. Raddatz, C. Thoben, S. Zimmermann, A compact high resolution electrospray ionization ion mobility spectrometer, Talanta 150 (2016) 1–6.
[15] Y. Du, H. Cang, W. Wang, F. Han, C. Chen, L. Li, K. Hou, H. Li, Note: design and construction of a simple and reliable printed circuit board-substrate bradbury-nielsen gate for ion mobility spectrometry, Rev. Sci. Instrum. 82 (8) (2011) 086103.
[16] J. Langejuergen, M. Allers, J. Oermann, A. Kirk, S. Zimmermann, High kinetic energy ion mobility spectrometer: quantitative analysis of gas mixtures with ion mobility spectrometry, Anal. Chem. 86 (14) (2014) 7023–7032.
[17] C.L. Crawford, H.H. Hill, Comparison of reactant and analyte ions for 63nickel, corona discharge, and secondary electrospray ionization sources with ion mobility-mass spectrometry, Talanta 107 (2013) 225–232.
[18] A.T. Kirk, M. Allers, P. Cochems, J. Langejuergen, S. Zimmermann, A compact high resolution ion mobility spectrometer for fast trace gas analysis, Analyst 138 (18) (2013) 5200–5207.
[19] H. Borsdorf, H. Schelhorn, J. Flachowsky, H.-R. Döring, J. Stach, Corona discharge ion mobility spectrometry of aliphatic and aromatic hydrocarbons, Anal. Chim. Acta 403 (1–2) (2000) 235–242.
[20] W. Vautz, A. Michels, J. Franzke, Micro-plasma: a novel ionisation source for ion mobility spectrometry, Anal. Bioanal. Chem. 391 (7) (2008) 2609–2615.
[21] P. Cochems, M. Runge, S. Zimmermann, A current controlled miniaturized non-radioactive electron emitter for atmospheric pressure chemical ionization based on thermionic emission, Sens. Actuat. A Phys. 206 (2014) 165–170.
[22] T. Reinecke, A.T. Kirk, A. Heptner, D. Niebuhr, S. Böttger, S. Zimmermann, A compact high-resolution X-ray ion mobility spectrometer, Rev. Sci. Instrum. 87 (5) (2016) 053120.
[23] C. Wu, W.F. Siems, G.R. Asbury, H.H. Hill, Electrospray ionization high-resolution ion mobility spectrometry-mass spectrometry, Anal. Chem. 70 (23) (1998) 4929–4938.